

Magnetic structure and diffracted magneto-optics of patterned amorphous multilayersUnnar B. Arnalds,¹ Evangelos Th. Papaioannou,¹ Thomas P. A. Hase,² Hossein Raanaei,³ Gabriella Andersson,¹ Timothy R. Charlton,⁴ Sean Langridge,⁴ and Björgvin Hjörvarsson¹¹*Department of Physics and Astronomy, Uppsala University, P.O. Box 516, 751 20 Uppsala, Sweden*²*Department of Physics, University of Warwick, Coventry CV4 7AL, United Kingdom*³*Department of Physics, Persian Gulf University, Bushehr 75168, Iran*⁴*ISIS, Harwell Science and Innovation Campus, Science and Technology Facilities Council, Rutherford Appleton Laboratory, Oxon OX11 0QX, United Kingdom*

(Received 10 June 2010; revised manuscript received 30 September 2010; published 25 October 2010)

We present magneto-optical Kerr effect measurements of patterned arrays of $\text{Co}_{68}\text{Fe}_{24}\text{Zr}_8/\text{Al}_2\text{O}_3$ amorphous multilayers. The multilayers were patterned in two dimensions into two different arrangements of circular and ellipsoidal islands. Magnetization loops were recorded in a longitudinal geometry using both the specularly reflected beam as well as diffracted beams scattered off the patterned films. The magnetization of the patterned structures is significantly different from the magnetization of a continuous multilayer owing to the lateral confinement of the pattern and the introduction of additional dipolar coupling between the layers at the edges of the islands. By investigating the magnetic response at the different diffraction orders from the two different configurations of islands we are able to observe the magnetization at different length scales and determine the magnetic response of the circular and ellipsoidal islands individually.

DOI: [10.1103/PhysRevB.82.144434](https://doi.org/10.1103/PhysRevB.82.144434)

PACS number(s): 75.70.Ak, 75.50.Kj, 68.65.Ac, 75.60.Jk

I. INTRODUCTION

Magnetism in artificially created microsized and nano-sized structures has been a growing field of research in recent years due mostly to the introduction and development of lithographic patterning techniques.^{1,2} Studies of patterned magnetic structures revolve around investigating the effect of the shape and size of the patterns as well as the influence of the layer thickness on the magnetic behavior.^{3,4} A large number of different configurations have been investigated such as stripes,⁵ dots, and rings of different sizes.^{6,7} So far most of the studies on patterned magnetic structures have been focused on single magnetic layers of isotropic materials, such as permalloy.^{8,9} Recently, however, there has been a growing interest in moving away from the single-layer paradigm and investigating patterned magnetic structures with more layers of different material combinations. In the case of multilayers, patterning introduces an additional interaction between the layers through the dipolar stray field along the edges of the patterned structures. This has, for example, been realized in spin chainlike structures¹⁰ and in circular multilayers with an odd number of dipole-coupled magnetic layers¹¹ and been observed to suppress vortex formation and make single-domain states more favorable.¹² In these cases, the interaction through the stray field modifies the magnetic alignment in each layer of the patterned multilayer when compared to the continuous sheet material. Material parameters such as magnetic anisotropy and exchange coupling furthermore play an important role in the magnetic behavior of the patterned multilayered structures.^{13,14}

In this paper, we investigate the magnetic properties of patterned multilayers of ferromagnetic and nonmagnetic layers in a combined structure of circular and ellipsoidal islands with the magneto-optical Kerr effect (MOKE); by Kerr microscopy and specular and diffracted MOKE measurements. For this study we choose amorphous $\text{Co}_{68}\text{Fe}_{24}\text{Zr}_8$ for the

ferromagnetic layer spaced with amorphous Al_2O_3 , thick enough to remove any direct coupling between the magnetic layers. Amorphous materials are extremely interesting since they can be considered to be isotropic and exhibit good layer perfection.¹⁵ In our case the layers were grown under the influence of a magnetic field, which for $\text{Co}_{68}\text{Fe}_{24}\text{Zr}_8$ gives rise to an imprinted uniaxial anisotropy due to small deviations from uniformity in the magnetization inherent in the material.¹⁶ The influence of shape and multilayer effects, growth-induced anisotropies, element arrangement, and direction of the applied field on the observed magnetization, in conjunction with micromagnetic simulations, are studied. The magnetization loops were recorded separately on the specularly reflected and diffracted beams in a longitudinal MOKE geometry. Measurements of the Kerr rotation, θ_K , of the specularly reflected beam in this geometry reveal the magnetization vector, M_x , parallel to both the sample plane and the applied field direction, averaged over the area illuminated by the laser spot. Diffracted MOKE magnetization loops, on the other hand, are proportional to the magnetic form factor f_n^m observed at the n th diffraction order of the scattered beam and can therefore yield information about the internal magnetization distribution of patterned elements in periodic arrays.^{17–24} Furthermore, they can also be used to investigate and compare patterns from different arrangements of the same elements as is demonstrated in this study.

II. EXPERIMENT

The multilayers were grown at room temperature on Si substrates, prepatterned by electron-beam lithography at the Micro and Nanotechnology Centre, STFC, using a double-layered polymethyl methacrylate electron-sensitive resist. By using a lower layer which is more sensitive to the electron exposure an overhang edge profile is created in the patterned resist, which reduces crowning, resulting in better layering of

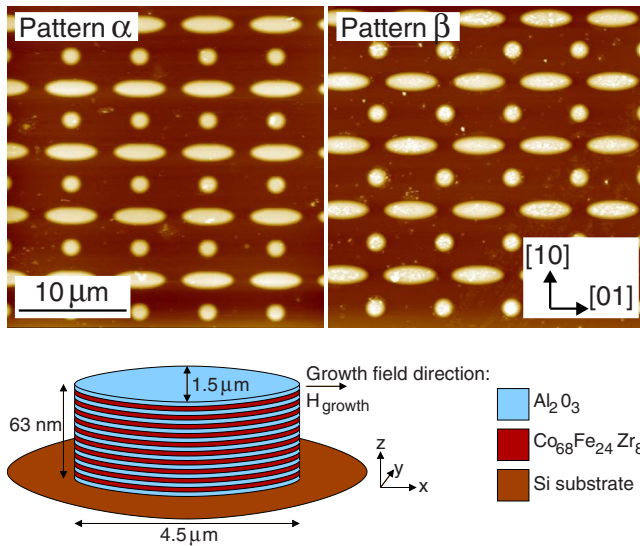


FIG. 1. (Color online) Atomic force microscopy images showing the patterns used in this investigation. The circular islands have a diameter of $1.5 \mu\text{m}$ and the ellipsoidal islands a $1.5 \mu\text{m}$ minor axis and a $4.5 \mu\text{m}$ major axis. The shortest distance between the edges of the islands is $1.5 \mu\text{m}$ resulting in a periodicity of $6 \mu\text{m}$ for both patterns along both the $[01]$ and $[10]$ lattice directions, defined in the inset.

the multilayer islands at their edges. With this procedure the multilayers were patterned into two different arrangements of $1.5\text{-}\mu\text{m}$ -diameter circular islands and $1.5 \times 4.5 \mu\text{m}^2$ ellipsoidal islands (see Fig. 1). In pattern α the circular islands are arranged to be in line with the minor axis of the ellipses whereas in pattern β they are shifted to be in the center of the ellipsoidal island sublattice.

The multilayers consisted of ten repetitions of 3-nm-thick $\text{Co}_{68}\text{Fe}_{24}\text{Zr}_8$, grown using dc magnetron sputtering and 3-nm-thick Al_2O_3 , grown using rf magnetron sputtering.^{15,25} To protect the magnetic layers from oxidation the sample stack started and ended with 3-nm-thick Al_2O_3 layers resulting in a total multilayer thickness of 63 nm. An Ar sputtering gas of purity 99.9999% and pressure 3.0 mTorr was used during deposition. The Ar gas was transferred through a chemical getter before entering the sputtering chamber. Before growth the base pressure of the growth chamber was below 2×10^{-7} Pa.

During growth an external magnetic field, H_{growth} , was applied parallel to the substrate using two flat permanent magnets mounted on a custom built sample holder described in detail elsewhere.¹⁵ Due to size constraints of the sample holder a position-dependent divergence in the growth field occurs over the $2 \times 2 \text{ cm}^2$ substrate area, although it is reasonably parallel over the central region. When grown under a magnetic field a uniaxial anisotropy, K_u , is imprinted into $\text{Co}_{68}\text{Fe}_{24}\text{Zr}_8$ defining an easy axis in the material along the growth field direction and a hard axis perpendicular to it.¹⁵

The prepatterned substrates were arranged so that the major axis of the ellipsoidal islands was parallel to the growth field. The use of elliptically shaped patterns introduces an easy magnetic axis along the major axis due to shape anisotropy. By this alignment the imprinted anisotropy, K_u , and

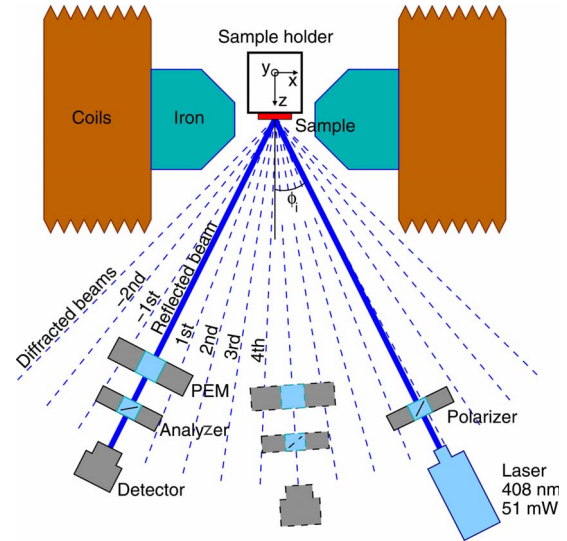


FIG. 2. (Color online) Schematic drawing showing the longitudinal MOKE setup for recording magnetization loops at specularly reflected and diffracted beams. The applied magnetic field was aligned to the x axis and the sample plane and the plane of incidence parallel to the xy and xz planes, respectively.

the shape anisotropy, K_s , of the ellipsoidal structures are parallel. In the case of the circular islands no shape anisotropy is expected so the easy axis is only defined by K_u . It should be noted that since the shape anisotropy due to the thickness of the films is much larger than the imprinted uniaxial anisotropy, the magnetization is forced to be in the sample plane. This holds even after patterning since the lateral dimensions of the islands are much larger than the thickness of the individual magnetic layers, as well as the thickness of the entire multilayer.

The layer thickness and interface roughness from the samples were determined using grazing incidence x-ray scattering. Specular reflectivity was recorded from the patterned samples on station X22C at the National Synchrotron Light Source (NSLS) at Brookhaven National Laboratory using a beam with an energy of 8.8 keV. The instrument resolution was defined by a set of incident slits with dimensions $150 \mu\text{m} \times 1 \text{ mm}$ and the scattered signal recorded in a slit-collimated scintillator detector with matched resolution. An automatic calibrated attenuator system was used to keep the count rate at the detector within its linear-response range, thereby avoiding saturation effects.

Magnetization loops were recorded using a longitudinal MOKE setup,²⁶ modified for diffracted MOKE measurements and depicted in Fig. 2. The longitudinal Kerr magnetometer, based on the use of a photoelastic modulator (PEM) operating at 50 kHz, allowed the measurement of the change in the polarization state of the reflected light. Through the measurement of the Kerr angle θ_K and ellipticity η of the reflected light the in-plane component of the magnetization M_x parallel to the applied field could be determined. The polarization state of the incident light, set by the first polarizer, corresponded to s -polarized light. The reflected beam passed through the PEM and a polarization analyzer before being measured by a photodetector. The retardation axis of

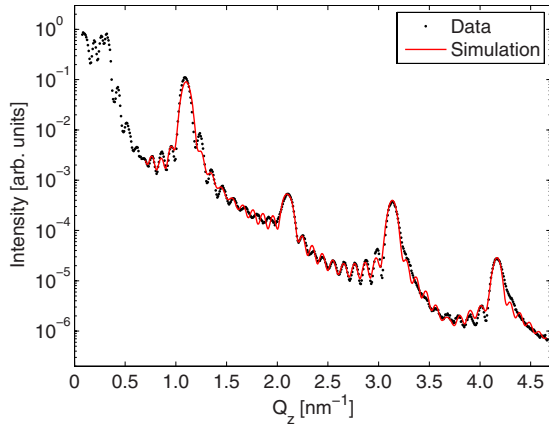


FIG. 3. (Color online) Specular x-ray reflectivity and simulation for pattern α recorded at an energy of 8.8 keV. Layer thicknesses are found to be in excellent agreement with the nominal growth parameters.

the PEM was aligned to be parallel to the plane of incidence. The analyzer was oriented at 45° with respect to the PEM retardation axis and the first polarizer to obtain a linear dependence between θ_K and the magnetization.²⁷ The measurements were performed with a 51 mW laser at a wavelength of $\lambda=408$ nm and an incidence angle of $\phi_i=24^\circ$ with respect to the sample surface normal. The high-intensity laser and the high modulation frequency of the PEM, combined with phase-sensitive amplification, allowed an accurate and sensitive registration of magnetization loops, even for low-intensity-diffracted beams.

Realspace imaging of the in-plane magnetization of the patterns was performed using Kerr microscopy.²⁸ Oblique white light was used with the incidence of the light and the polarizers configured so that the magnetic contrast was sensitive to magnetization components along the lateral direction in the images. An averaged background image was recorded in an alternating magnetic field, and this background was then subtracted from subsequently recorded images. This results in a purely magnetic black and white contrast. The images were recorded in zero applied field, after letting the amplitude of an alternating magnetic field decline over a time of 20 s.

III. RESULTS

A. Structural characterization

The specular x-ray reflectivity from sample α is shown in Fig. 3. The specular scattering from these patterned multilayers is the incoherent sum of two terms; first that arising from the patterned multilayered islands and second that associated with the surrounding bare substrate. Fortunately, the latter has a faster intensity fall-off with scattering angle and only acts as a background signal in the data. The analysis of the data is complicated further by the presence of both the zero-order scattering from the patterned multilayer and the scattering arising from the average surface. For this particular sample these two effects combine to make alignment of the sample difficult for low-scattering angles and consequently

the data presented in Fig. 3 has only been fitted above $Q_z=0.7$ nm⁻¹. Normally the forward diffuse scattering (which also occurs at the specular condition) can be removed by subtracting an off-set Q_z longitudinal diffuse scan, but in this case the presence of the lateral pattern introduces additional sharp peaks as a function of Q_x which are close to the specular condition making this unfeasible. However, the diffuse scattering was observed to be low and is incorporated into our model as a small constant background. The reflectivity was fitted to a simple model, and we have concentrated on elucidating the multilayer parameters as these are much less prone to the systematic errors eluded to previously. The best-fit simulations derived using a differential evolution algorithm and a figure of merit parameter based on a χ^2 minimization²⁹ is shown as the solid line in Fig. 3 and matches the data well. The fitted layer thicknesses are in good agreement with the nominal growth parameters with $d_{\text{Al}_2\text{O}_3}=3.12(4)$ nm and $d_{\text{Co}_{68}\text{Fe}_{24}\text{Zr}_8}=2.91(4)$ nm. The low level of diffuse scattering suggests smooth interfaces with a low topological roughness amplitude which is in agreement with the total interface widths deduced from the specular fit. Within the multilayer, growth of Al₂O₃ onto Co₆₈Fe₂₄Zr₈ results in a smoother interface, with a roughness of $\sigma_{\text{Al}_2\text{O}_3}=0.44(2)$ nm, than when Co₆₈Fe₂₄Zr₈ is deposited onto Al₂O₃, having a roughness of $\sigma_{\text{Co}_{68}\text{Fe}_{24}\text{Zr}_8}=0.68(2)$ nm.

B. Magnetic characterization

The magnetization component, M_x , was recorded with MOKE measurements at the specularly reflected beam for both patterns. Furthermore, magnetization loops were recorded for a continuous multilayer, of the same multilayer structure, along the easy and hard axes defined by the imprinted anisotropy. Figures 4(a) and 4(b) show MOKE magnetization loops recorded for the continuous multilayer. The easy-axis magnetization loop is square with 100% remanence and a coercivity of $\mu_0 H_c=1.4$ mT, while the hard axis exhibits a linear magnetization curve with small coercivity, almost zero remanence and saturation at $\mu_0 H=\pm 8$ mT. These results compare closely to magnetization loops recorded for single layers of Co₆₈Fe₂₄Zr₈, indicating a negligible coupling between the magnetic layers.

After patterning a completely different magnetization behavior emerges (when compared with the continuous multilayer). Figures 4(c) and 4(d) show specularly reflected MOKE magnetization loops recorded for pattern α . For the [01] direction a sharp transition at low field and a smooth transition extending up to saturation at $\mu_0 H \approx \pm 30$ mT are invoked. For the [10] direction both the imprinted uniaxial anisotropy and the structural anisotropy of the ellipsoidal islands are expected to have a hard axis, resulting in a higher saturation field, observed to be $\mu_0 H \approx \pm 45$ mT. Differences between the magnetization loops recorded for the two different patterns should indicate if magnetostatic coupling between the islands is affecting their magnetization reversal. Only minor differences were observed for the magnetization loops recorded for patterns α and β . No interaction between the islands can be inferred since misalignment of the growth field can also be responsible for any of the observed differ-

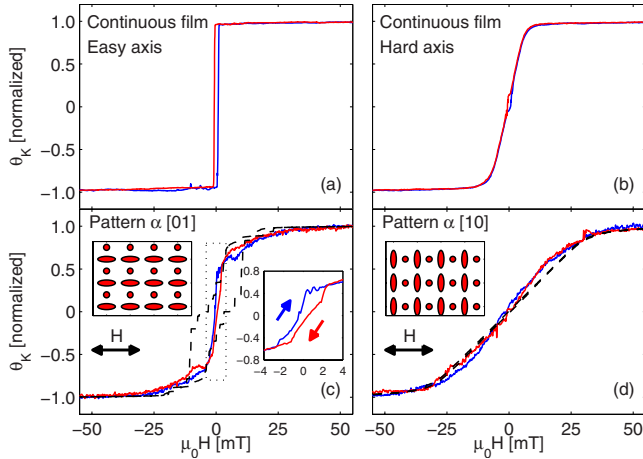


FIG. 4. (Color online) MOKE magnetization loops of a continuous multilayer film for the (a) easy and (b) hard directions of the imprinted anisotropy and for pattern α along the (c) [01] and (d) [10] lattice directions (similar results were obtained for pattern β). An inverted hysteresis, shown in the inset in graph (c), is observed at low fields and attributed to the demagnetizing field between layers. Blue and red lines (dark gray and light gray) represent the magnetization under increasing or decreasing applied magnetic field, respectively. The Kerr rotations for all the measured curves are normalized to their respective maximum values. The dashed lines in (c) and (d) show results of micromagnetic calculations.

ences. These results do not remove the possibility of coupling between the islands but indicate that it does not affect strongly the overall magnetization behavior of the islands.

The magnetic behavior of the circular and ellipsoidal multilayer islands as a function of magnetic field was simulated using the object oriented micromagnetic framework (OOMMF).³⁰ The calculations were carried out for individual circular and ellipsoidal multilayer islands thereby excluding any magnetostatic interactions between adjacent islands. Each island consisted of ten repetitions of 3-nm-thick magnetic layers spaced with 3-nm-thick nonmagnetic layers. The values for the saturation magnetization, M_s , and uniaxial anisotropy, K_u , used for the calculations were determined experimentally for $\text{Co}_{68}\text{Fe}_{24}\text{Zr}_8$ continuous multilayers. From superconducting quantum interference device measurements the saturation magnetization was determined to be $M_s = 900$ kA/m. Magnetization loops recorded for continuous multilayers, shown in Figs. 4(a) and 4(b), were used to determine the imprinted uniaxial anisotropy to be $K_u = 3.5$ kJ/m³.³¹ The exchange constant was not observed to have a strong effect on the results of the simulations so a value of $A = 30 \times 10^{-12}$ J/m, corresponding to the exchange constant of Co, was used. In the simulations the circular and ellipsoidal islands were discretized into cells with dimensions of $20 \times 20 \times 3$ nm³. The calculations were performed for each field value in steps of 0.2 mT until the stopping criteria of $|\mathbf{dm}/dt| < 0.17^\circ/\text{ns}$ for all spins in the simulated structure was reached. Due to the large size and multilayer nature of the islands the number of individual cells was limited by computational time. Such a large cell size, compared to the exchange length of $l_{ex} = 5.4$ nm for the experimental parameters used, results in an underestimation of the ex-

change interaction. Furthermore, short-length scale phenomena, such as vortex formation, cannot be accounted for using such a large cell size. From the simulations it was, however, determined that the cell size was small enough to obtain a reasonably realistic result with the maximum observed angle between the magnetization orientation of neighboring spins always lying below 22° . They can therefore be considered to yield insight into the magnetic structure of the islands. The calculated curves, shown with dashed lines in Figs. 4(c) and 4(d), represent a summation of the magnetization along the x axis, M_x , for all the layers in the structures with the results from the circular and ellipsoidal structures added together. Given the limitations of the simulations the results are in good agreement with the measurements. The calculated magnetization loops show similar saturation field values and general reversal behavior as the specular MOKE measurements. Along the easy axis, steps in the magnetization loops were observed in the calculations for both the circular and ellipsoidal islands due to the switching of individual layers within the multilayers at different field values. Such a pronounced steplike behavior is not observed in the measured loops. This discrepancy is attributed to the measured loops being a statistical average of the magnetic state in a large number of individual magnetic islands at a finite temperature. Neither of these effects are taken into account in the calculations. The large cell size used may also introduce an amplification of their effects in the magnetization reversal. For the hard axis a smooth magnetization rotation is observed indicating a smooth variation in the magnetization of individual layers. For both in-plane array directions, an antiferromagnetic arrangement between adjacent layers in the multilayer stack is formed as the external field is reduced to 0 mT due to the demagnetizing effect of the dipole interaction between the layers. Figure 5 shows the magnetization vectors for individual layers of the circular islands, obtained from the micromagnetic calculations, for selected values of the applied field. The magnetization vectors are shown for both the easy and hard axes directions. For the easy axis the reduction in the net magnetic moment, as the applied field tends to zero, is a consequence of the individual layers switching through spin-flop transitions at different field values whereas for the hard axis the reduction is a manifestation of the individual layers rotating out of the applied field direction toward the easy axis defined by the imprinted uniaxial anisotropy, K_u . Micromagnetic simulations for the ellipsoidal islands exhibited similar magnetic behavior.

Figure 6 shows a Kerr microscope image of the remanent magnetization for pattern α along the [01] direction. From the image a distinct single-domain remanent signal is observed for the magnetization of the ellipsoidal islands. No preferred orientation of the magnetization in the ellipsoidal islands is seen indicating that dipole coupling between individual ellipsoidal islands does not have an observable effect. Furthermore, differences can be seen in the grayscale values of the circular islands indicating that they too have a remanent magnetization, but the signal strength is too weak for a quantitative analysis.

The sharp transition, seen in Fig. 4(c), for the [01] direction exhibits an inverted hysteresis. This inverted hysteresis was observed for both patterns as well as measurements per-

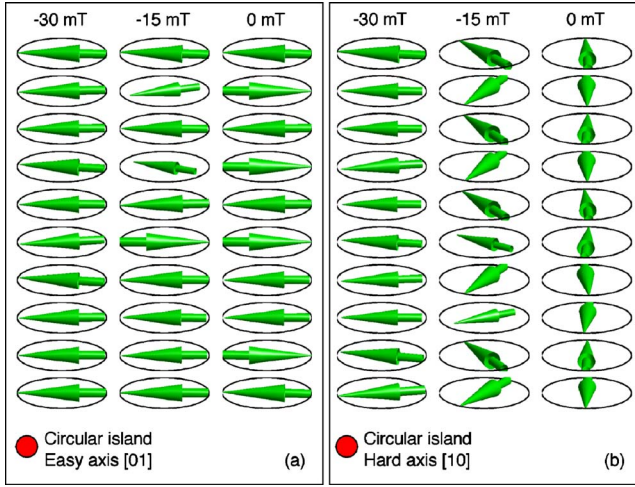


FIG. 5. (Color online) Results of micromagnetic calculations for individual circular islands for (a) the easy-axis direction and (b) the hard-axis direction. The arrows show the net magnetization vector for individual layers. The circles surrounding the magnetization vectors correspond to the maximum magnetization possible for each layer. In both cases an antiferromagnetic arrangement occurs between the layers. At remanence the magnetization vectors align to the easy axis. This is illustrated in (b) where an arrangement perpendicular to the applied field direction occurs.

formed at different incidence angles within the angular range of the MOKE setup, $\phi_i = 10^\circ$ to $\phi_i = 45^\circ$. Inverted hysteresis loops have been previously observed in numerous cases, for example, multilayer structures with out-of-plane magnetization and antiferromagnetic coupling as well as molecular magnets.^{32–34} The dipole coupling at the edges of the structures investigated here gives rise to demagnetizing fields between the layers, resulting in an antiferromagnetic arrangement of the magnetization of the layers at low-field values. The layers at the extremity of the multilayer stack lack neighbors and therefore experience a weaker dipole coupling.¹⁰ They thereby align more easily to the applied field. The antiferromagnetic arrangement between adjacent layers in the multilayer therefore starts to form from the center of the stack, as the field is decreased toward zero (see Fig. 5). For optical wavelengths the intensity of the light in the sample decays exponentially with depth resulting in a limited penetration depth of the MOKE technique.^{15,35} This affects

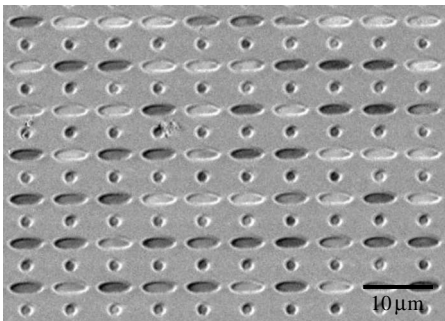


FIG. 6. Kerr microscopy image showing the remanent magnetization of pattern α after the field was applied along the [01] direction.

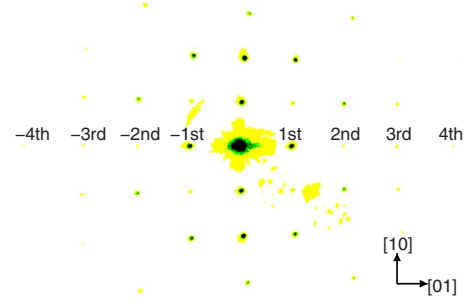


FIG. 7. (Color online) A picture showing the distribution of diffraction spots for pattern α with the [01] direction parallel to the plane of incidence. Magnetization loops were recorded at the specularly reflected beam and at positive diffraction orders on the [01] and [10] principal axes.

the observed magnetization since layers closer to the surface of the multilayer will contribute more to the measured signal than lower lying layers and therefore a magnetization that does not correspond to the average magnetization is observed. Assuming optical constants for Co (Ref. 36) the penetration depth of the light used in this MOKE setup can be estimated to be approximately four magnetic layers. If the magnetization of the layers is not aligned ferromagnetically the penetration depth of the light influences the recorded magnetization signal resulting in the possibility of observing an inverted hysteresis due to the demagnetizing field of the lower lying layers.

C. Diffracted MOKE characterization

To examine the internal magnetization distribution of these patterns we utilize magnetization loops recorded at diffraction peaks along the principal axes (see Fig. 7). Magnetization loops recorded using beams diffracted from patterned surfaces are proportional to the magnetic form factor f_n^m .^{18,37} The magneto-optical signal as a function of diffraction order, n , in a longitudinal geometry is given by^{18,20,37}

$$f_n^m = \int_S m(x) \exp(in\mathbf{G} \cdot \mathbf{r}) dS, \quad (1)$$

where, in our case, the integration is carried out over the two-dimensional unit cell of the periodic array, \mathbf{G} is the reciprocal lattice vector, and $m(x)$ is the magnetization component parallel to the external field. Given that the patterns used in this study are individual sublattices of circular and ellipsoidal islands a simple analysis can be performed by considering each structure to have independent magnetic form factors. If $f_{n,c}^m$ and $f_{n,e}^m$ are the magnetic form factors for the circular and ellipsoidal islands, respectively, the total magnetic form factor is then

$$f_n^m = f_{n,c}^m + f_{n,e}^m, \quad (2)$$

where in each case the integration in Eq. (1) is carried out over unit cells of the circular and ellipsoidal island sublattices. Since both patterns α and β have the same periodicity, and assuming that the interdot coupling is weak, such that individual islands have the same magnetization distribution

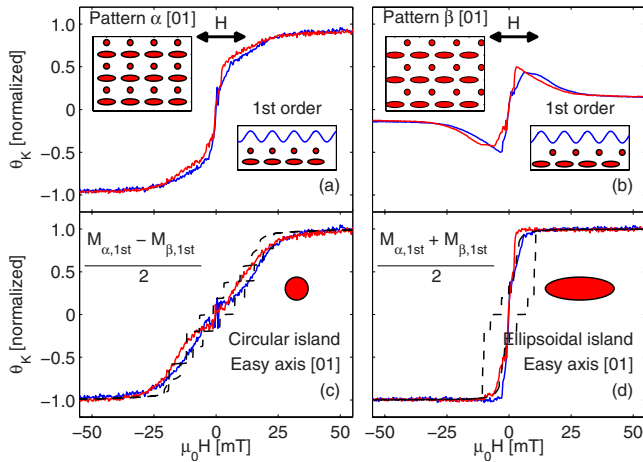


FIG. 8. (Color online) [(a) and (b)] The first-order magnetization loops for patterns α and β along the [01] direction. (c) The magnetization of the circular islands obtained from the difference between the magnetization of patterns α and β . (d) The magnetization of the ellipsoidal islands obtained from the average of the first-order magnetizations. The Kerr rotation for all the measured curves is normalized to their respective saturation value except for the curve in (b) which is scaled according to results of numerical Fourier transform calculations. The dashed lines in (c) and (d) show results of micromagnetic calculations for the magnetization of individual structures. The insets in (a) and (b) show a standing-wave model illustrating the inversion of the circular island form factor between the two patterns.

irrespective of the pattern, we can state that the ellipsoidal islands can be considered to have the same magnetic form factors for each pattern. For the circular islands along the [10] direction a shift of the phase factor for the circular island form factor $f_{n,c}^m$ by $e^{in\pi}$ is expected due to the lateral shift of the circular island sublattice by half the periodicity between the two patterns, α and β . Therefore an inverted form factor should be observed for odd-number diffraction orders between the two different patterns along this direction. The individual magnetizations, $M_{c[01]}$ and $M_{e[01]}$, of the sublattice unit cells, for the circular and ellipsoidal islands, respectively, can therefore be obtained by comparing the two magnetization loops after scaling their intensity to the form factor of each pattern, obtained by numerical Fourier transform calculations. Magnetization loops recorded at the first positive diffraction order (see Fig. 2) for patterns α and β along the [01] direction are shown in Figs. 8(a) and 8(b). Since the observed magnetization is proportional to the magnetic form factor the difference between the two scaled curves yields the magnetization of the circular islands, $M_{c[01]}$, [shown in Fig. 8(c)] as the magnetization of the ellipsoidal islands, $M_{e[01]}$, is canceled by this operation. When the two curves in Figs. 8(a) and 8(b) are averaged the magnetization of the circular islands, $M_{c[01]}$, is canceled revealing the magnetization of the ellipsoidal islands, $M_{e[01]}$, shown in Fig. 8(d). The magnetization of the individual islands obtained with this method correspond closely to the micromagnetic simulations for individual circular and ellipsoidal islands shown with dashed lines in Figs. 8(c) and 8(d).

Magnetization loops for the [10] direction, recorded at the first and second diffraction orders, are shown in Figs. 9(a)

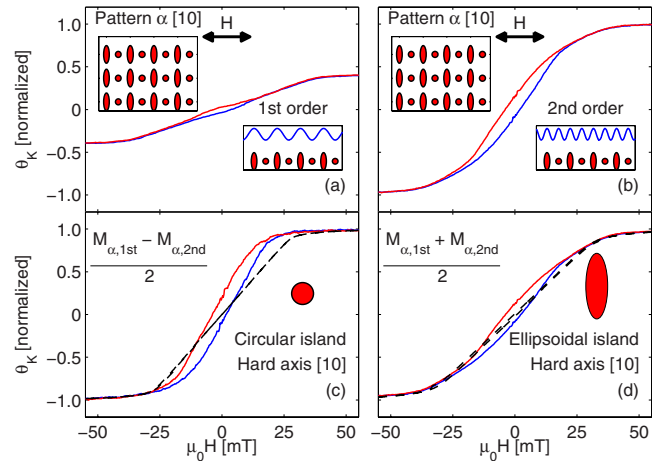


FIG. 9. (Color online) [(a) and (b)] The first- and second-order magnetization loops for pattern α along the [10] direction. (c) The magnetization of the circular islands obtained from the difference between the first- and second-order magnetization. (d) The magnetization of the ellipsoidal islands obtained from the average of the first- and second-order magnetization. The dashed lines in (c) and (d) show results of micromagnetic calculations for the magnetization of individual structures. Similar results were obtained for pattern β .

and 9(b). To obtain the magnetization of the individual islands for this direction, a similar method can be applied observing the inversion of the form factor of the circular islands between the first and second diffraction orders. Such a method has been previously reported for patterned single-layered Fe films.³⁸ For this method, however, the form factors and length scales for the two diffraction orders are different so a less exact result is obtained. As before, the curves are scaled according to results of numerical Fourier transform calculations. The difference between the magnetization loops recorded at the first and second diffraction orders reveals the magnetization of the circular islands, shown in Fig. 9(c), while the average of the two curves can be used to obtain the magnetization of the ellipsoidal islands, shown in Fig. 9(d). The magnetization of the ellipsoidal islands obtained with this method correspond closely to the micromagnetic calculations. However, in the case of the magnetization of the circular islands a higher saturation value is observed in the simulations. Furthermore, the magnetization loops for both the circular and ellipsoidal islands exhibit a hysteresis which is not accounted for in the simulations.

Magnetization loops were recorded at higher order diffraction peaks for both patterns showing strong variations between the different diffraction orders (see Fig. 10). For both the [01] and [10] directions similar magnetization loops are observed for the different diffraction orders for both patterns. For the [01] direction the phase shift of the circular islands between the patterns appears to not affect the recorded signal at these diffraction orders. At the second-order diffraction an inversion of the signal from the ellipsoidal islands is observed due to a reduced, negative form factor for the ellipses compared to the first order. At the third diffraction order for the [01] direction the recorded loops reveal the magnetization of the ellipses to be severely reduced due to a

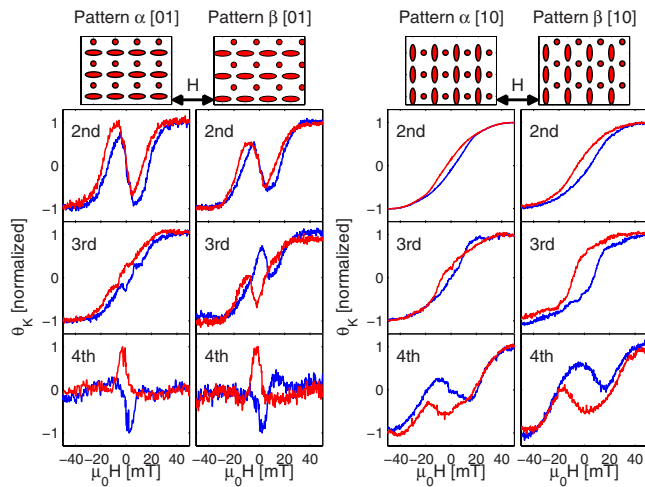


FIG. 10. (Color online) Magnetization loops recorded at the second, third, and fourth diffraction order for both patterns α and β measured with field and magnetization along both the $[01]$ and $[10]$ directions.

negligible form factor, $f_{3,e}^m$. The magnetization recorded at the third diffraction order, therefore corresponds closely to the magnetization of the circular islands, shown in Fig. 8(c). At the fourth diffraction order the corresponding length scale is the same as the diameter of the circular islands resulting in reduced form factors for both structures. At this diffraction order divergences of the magnetization at the edges of the islands are therefore enhanced. A similar hump is observed for both patterns indicating that a nonlinear variation is contributing to the signal and enhanced at this diffraction order. Dipole coupling between layers of the islands induces a divergence of the dipole field of each layer causing the magnetization of the layers to deviate. These effects were observed in the micromagnetic simulations to be predominantly at the edges of the elements and therefore they should be more pronounced at higher order diffraction, as can be seen in the magnetization loops for the third- and fourth-order diffraction peaks. In order to fully describe these deviations using diffracted MOKE measurements the magnetic behavior would need to be determined at still higher diffraction orders in order to access shorter length scales. Unfortunately, these higher orders are not easily accessible using visible light.

For the $[10]$ direction strong variations are also observed in the magnetization loops recorded at each of the higher diffraction orders. Similar loops are obtained for the two different arrangements at the second and fourth diffraction

order while the third diffraction order shows slightly different loops with an enhanced opening for pattern β . For this direction the micromagnetic calculations revealed a strong divergence as the magnetizations of the individual layers rotated toward an antiferromagnetic alignment which is strongly enhanced at the fourth diffraction order.

IV. SUMMARY AND CONCLUSIONS

In this work we have applied magneto-optical measurements to obtain information about the magnetization of two-dimensionally patterned multilayers. For the samples investigated in this study several factors contribute to the observed magnetization behavior such as the imprinted anisotropy, shape anisotropy, and the dipole coupling between layers. From specular MOKE measurements we are able to obtain information on the average magnetization in these samples. However, through such measurements the magnetic structure of the whole multilayer stack cannot be determined, since the magnetization of individual layers is averaged out owing to the wavelength of the optical light being orders of magnitude longer than the periodicity of the multilayers. The limited penetration depth of MOKE measurements therefore plays a strong role, enhancing the contribution of magnetic layers closer to the surface of the multilayer, giving rise to an observed inverted hysteresis. Using diffracted MOKE measurements we have determined the lateral magnetic structure and the magnetization of individual islands within the patterns. These results therefore show that magnetic information carried with beams, specularly reflected and diffracted, from patterned magnetic multilayers can be used to determine the magnetic structure of complicated three-dimensional structures.

ACKNOWLEDGMENTS

The authors would like to acknowledge the support of the Swedish Research Council (VR) and the Knut and Alice Wallenberg Foundation (KAW) and funding from the Icelandic Nanoscience and Nanotechnology program and the Icelandic Research Fund for Graduate Students. We would furthermore like to express our thanks to S. B. Wilkins for the excellent support received during data collection at the NSLS and gratefully acknowledge discussions with Min-Sang Lee. Use of the National Synchrotron Light Source, Brookhaven National Laboratory, was supported by the U.S. Department of Energy, Office of Science, Office of Basic Energy Sciences, under Contract No. DE-AC02-98CH10886.

¹J. I. Martín, J. Nogués, K. Liu, J. L. Vicent, and I. K. Schuller, *J. Magn. Magn. Mater.* **256**, 449 (2003).

²A. O. Adeyeye and N. Singh, *J. Phys. D: Appl. Phys.* **41**, 153001 (2008).

³R. P. Cowburn, *J. Phys. D* **33**, R1 (2000).

⁴M. Schneider, H. Hoffmann, and J. Zweck, *Appl. Phys. Lett.* **77**, 2909 (2000).

⁵W. C. Uhlig and J. Shi, *Appl. Phys. Lett.* **84**, 759 (2004).

⁶T. Uhlig and J. Zweck, *Phys. Rev. Lett.* **93**, 047203 (2004).

⁷M. Kläui, C. A. F. Vaz, J. A. C. Bland, T. L. Monchesky, J. Unguris, E. Bauer, S. Cherifi, S. Heun, A. Locatelli, L. J. Heyderman, and Z. Cui, *Phys. Rev. B* **68**, 134426 (2003).

⁸X. Zhu, P. Grutter, V. Metlushko, and B. Ilic, *Appl. Phys. Lett.* **80**, 4789 (2002).

- ⁹P. Vavassori, G. Gubbiotti, G. Zangari, C. T. Yu, H. Yin, H. Jiang, and G. J. Mankey, *J. Magn. Magn. Mater.* **242-245**, 585 (2002).
- ¹⁰M. van Kampen, I. L. Soroka, R. Bručas, B. Hjörvarsson, R. Wieser, K. D. Usadel, M. Hanson, O. Kazakova, J. Grabis, H. Zabel, C. Jozsa, and B. Koopmans, *J. Phys.: Condens. Matter* **17**, L27 (2005).
- ¹¹A. A. Fraerman, B. A. Gribkov, S. A. Gusev, A. Yu. Klimov, V. L. Mironov, D. S. Nikitushkin, V. V. Rogov, S. N. Vdovichev, B. Hjörvarsson, and H. Zabel, *J. Appl. Phys.* **103**, 073916 (2008).
- ¹²Y. Choi, D. R. Lee, J. W. Freeland, G. Srajer, and V. Metlushko, *Appl. Phys. Lett.* **88**, 112502 (2006).
- ¹³V. Baltz, A. Bollero, B. Rodmacq, B. Dieny, J. P. Jamet, and J. Ferré, *Eur. Phys. J.: Appl. Phys.* **39**, 33 (2007).
- ¹⁴A. Bollero, B. Dieny, J. Sort, K. S. Buchanan, S. Landis, and J. Nogués, *Appl. Phys. Lett.* **92**, 022508 (2008).
- ¹⁵H. Raanaei, H. Nguyen, G. Andersson, H. Lidbaum, P. Korelis, K. Leifer, and B. Hjörvarsson, *J. Appl. Phys.* **106**, 023918 (2009).
- ¹⁶T. Hase, H. Raanaei, H. Lidbaum, C. Sánchez-Hanke, S. Wilkins, K. Leifer, and B. Hjörvarsson, *Phys. Rev. B* **80**, 134402 (2009).
- ¹⁷O. Geoffroy, D. Givord, Y. Otani, B. Pannetier, A. D. Santos, M. Schlenker, and Y. Souche, *J. Magn. Magn. Mater.* **121**, 516 (1993).
- ¹⁸M. Grimsditch and P. Vavassori, *J. Phys.: Condens. Matter* **16**, R275 (2004).
- ¹⁹A. Westphalen, M.-S. Lee, A. Remhof, and H. Zabel, *Rev. Sci. Instrum.* **78**, 121301 (2007).
- ²⁰M.-S. Lee, A. Westphalen, A. Remhof, A. Schumann, and H. Zabel, *J. Appl. Phys.* **103**, 093913 (2008).
- ²¹J. L. Costa-Krämer, R. Alvarez-Sánchez, A. Bengoechea, F. Torres, P. García-Mochales, and F. Briones, *Phys. Rev. B* **71**, 104420 (2005).
- ²²D. Jaque, J. I. Martín, G. Armelles, J. L. Costa-Krämer, F. Briones, and J. L. Vicent, *J. Appl. Phys.* **91**, 382 (2002).
- ²³T. Schmitte, K. Westerholt, and H. Zabel, *J. Appl. Phys.* **92**, 4524 (2002).
- ²⁴P. García-Mochales, J. L. Costa-Krämer, G. Armelles, F. Briones, D. Jaque, J. I. Martín, and J. L. Vicent, *Appl. Phys. Lett.* **81**, 3206 (2002).
- ²⁵A. Liebig, P. Korelis, H. Lidbaum, G. Andersson, K. Leifer, and B. Hjörvarsson, *Phys. Rev. B* **75**, 214202 (2007).
- ²⁶E. Th. Papaioannou, V. Kapaklis, P. Patoka, M. Giersig, P. Fumagalli, A. Garcia-Martin, E. Ferreira-Vila, and G. Ctistis, *Phys. Rev. B* **81**, 054424 (2010).
- ²⁷P. Q. J. Nederpel and J. W. D. Martens, *Rev. Sci. Instrum.* **56**, 687 (1985).
- ²⁸A. Hubert and R. Schäfer, *Magnetic Domains* (Springer, New York, 1998).
- ²⁹M. Björck and G. Andersson, *J. Appl. Crystallogr.* **40**, 1174 (2007).
- ³⁰M. J. Donahue and D. G. Porter, National Institute of Standards and Technology Interagency Report No. NISTIR 6376, 1999, <http://math.nist.gov/oommf>
- ³¹M. T. Johnson, P. J. H. Bloemen, F. J. A. den Broeder, and J. J. de Vries, *Rep. Prog. Phys.* **59**, 1409 (1996).
- ³²J. Hanmin, S. Dongsheng, G. Cunxu, and H. Kim, *J. Magn. Magn. Mater.* **308**, 56 (2007).
- ³³P. Pouloupoulos, R. Krishnan, and N. K. Flevaris, *J. Magn. Magn. Mater.* **163**, 27 (1996).
- ³⁴D. Belo, L. C. J. Pereira, M. Almeida, C. Rovira, J. Veciana, and V. Gama, *Dalton Trans.* **2009**, 4176.
- ³⁵E. Th. Papaioannou, M. Angelakeris, N. K. Flevaris, P. Fumagalli, Ch. Mueller, A. Troupis, A. Spanou, V. Karoutsos, P. Pouloupoulos, V. Kapaklis, and C. Politis, *J. Appl. Phys.* **101**, 023913 (2007).
- ³⁶*Handbook of Optical Constants of Solids*, edited by E. D. Palik (Academic Press, San Diego, 1991), Vol. 2.
- ³⁷M. Grimsditch, P. Vavassori, V. Novosad, V. Metlushko, H. Shima, Y. Otani, and K. Fukamichi, *Phys. Rev. B* **65**, 172419 (2002).
- ³⁸P. Vavassori, V. Metlushko, and M. Grimsditch, *Phys. Rev. B* **61**, 5895 (2000).